MICHIGAN STATE
UNIVERSITY

National Superconducting Cyclotron Laboratory

FRAGMENT DETECTION SYSTEM FOR STUDIES OF EXOTIC, NEUTRON-RICH NUCLEI

J.J. KRUSE, A. GALONSKY, C. SNOW, E. TRYGGESTAD,
J. WANG, K. IEKI, Y. IWATA and P.D. ZECHER

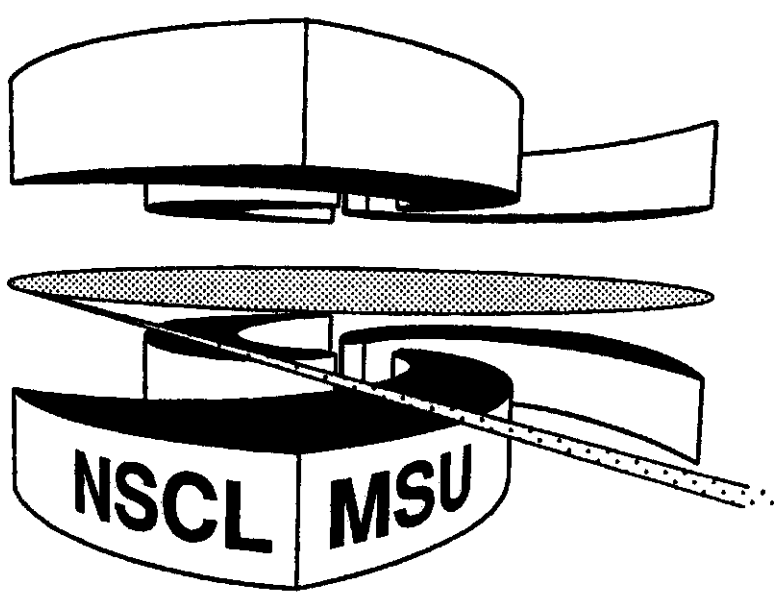

MSUCL-1181

OCTOBER 2000

Fragment detection system for studies of exotic, neutron-rich nuclei

J.J. Kruse[*a,b,1], A. Galonsky[a,b], C. Snow[a], E. Tryggestad[a,b], J. Wang[a,b,2], K. Ieki[c], Y. Iwata[c,3] and P.D. Zecher[a,b,4]

[a]*National Superconducting Cyclotron Laboratory, Michigan State University, East Lansing, Michigan 48824-1321*

[b]*Department of Physics and Astronomy, Michigan State University, East* Lansing, *Michigan 48824-*

[c]*Department of Physics, Rikkyo University, 3-Nishi-Ikebukuro, Toshima, Tokyo 171. Japan*

Abstract

We have developed a fragment detection system for use in studies of exotic, neutron-rich nuclei. Using a C-shaped dipole magnet, the system sweeps charged fragments and on-reacted beam particles through an angle before stopping them in an array of plastic scintillator detectors, recording time-of-flight and total energy, The system also includes a pair of silicon strip detectors to measure fragment angle of emergence from the target and energy loss for particle identification.

PACS: 29.40.Gx; *29.40. Mc;* 29.30.Aj

Keywords: Neutron-fragment coincidences; Fragment kinematics

* Corresponding author. Tel.: +1 507 266 6807, fax: cl 507 284 0079,

E-mail address: kruse.jon@mayo.edu

'Present address. Mayo Clinic Dep't of Radiation Oncology, 200 1st St. SW, Rochester, MN 55905, USA

'Present address. American Express Co., 3WFC,4712B, 200 Vesey St., New York, NY 10285, USA

[3]Present address. National Inst. of Radiological Sciences, 4-9-I Anagawa, Inage, Chiba 263-8555, Japan

[4] Present address. Investor Analytics LLC, 80 Broad Street, New York, NY 10004, USA

1. Introduction

Of all the isotopes available for study with the development of Radioactive Nuclear Beam facilities, none have received the attention given to ^{11}Li. After the first experiment of ^{11}Li in which the break-up neutrons were detected [1], a kinematically complete measurement of the Coulomb dissociation into a ^{9}Li fragment and two neutrons [2,3,4] was performed at the National Superconducting Cyclotron Laboratory (NSCL). The experimenters placed a Pb target in a beam of ^{11}Li nuclei of energy 30 MeV/nucleon. The electric field of the lead nucleus acted as a source of virtual photons capable of dissociating the ^{11}Li nucleus. By measuring the energy and

angle of the ^{9}Li and of each of the two neutrons, they were able to determine the energy of the absorbed photon for each dissociation event. A typical absorption released ~ 1 MeV, to be shared amongst the three decay products, giving each of them a velocity much smaller than the velocity of the ^{11}Li projectile. Consequently, all three of the reaction products left the target in a forward-focused cone. Because of this focusing effect, both the fragment and neutron detectors were centered at 0°.

The fragment detector was a Si/CsI telescope whose ΔE and E signals gave the Z, A and energy of the fragment. The angle of emission of the fragment was determined from the (x,y) signals in a double-sided strip detector traversed by the fragment. The E detector, a 1.2-cm thick CsI scintillator crystal, stopped all fragments and beam particles and also gave a timing signal as part of the system for determining the flight times of the two neutrons.

These neutrons were detected by an array of 54 cans of liquid scintillator located 5-6 m downstream from the target. Later, the cans were replaced by the NSCL Neutron Walls, a pair of 2m x 2m liquid scintillator arrays [4]. Neutron attenuation in the Si/CsI telescope was negligible, but neutron **production** was not. Approximately 1% of the ^{11}Li particles dissociated in the target, and another 1% dissociated in the Si/CsI telecsope. Most of the telescope events could not be distinguished from the target events, and so a significant portion of the beam time was devoted to running with no target, so that the contribution from the fragment detector could be measured and subtracted. Also, the dominant contribution to the width of the decay energy resolution came from the thickness of the target. Use of a thinner target would have improved the resolution, but would also have resulted in an even smaller dissociation rate, causing the experiment to be dominated by dissociations in the detector stack.

In order to eliminate or greatly reduce the background of dissociations in the fragment detector, a new system was developed. In this system, a thin silicon strip detector gives the fragment angle and ΔE signal. A beam-sweeping dipole magnet is placed between the target and the E detector, which is a set of plastic scintillators. If dissociation occurs in the target, the neutrons and the fragment leave the target in the forward direction, the neutrons traveling straight through the magnetic field to the neutron walls. The fragment, however, is swept by the magnetic field through an angle before being stopped in a scintillator. Unreacted beam particles are also swept through an angle before being stopped. If they dissociate in the E detector, the

neutrons are produced at a sufficient angle that they either miss, or can be shielded from, the neutron detector, eliminating these events as a source of background.

The components of the system are described in Sections 2, 3 and 4, the performance of the system in Section 5.

2. The beam-sweeping dipole

The magnet is a former beam-line dipole magnet from the Bevalac at Berkeley. It is a 7-ton, room temperature, C-shaped magnet with pole faces 33 cm wide x 61 cm long. The pole faces are surrounded on the entrance, exit, and the side opposite the return yoke by 18-cm wide coils. Neutrons from the target, which is at the entrance end of the magnet (see Figure 1), have about a 1-m path to the exit. The maximum vertical angle at which a neutron may leave the target without striking the pole faces or coils of the magnet is then determined by the pole gap, which was originally 15 cm. In order to increase this angle, or vertical input, an additional 3.8 cm of steel was inserted in the return yoke of the magnet, increasing the vertical gap to 19 cm and the vertical input from 8.7° to 11°. This, of course, reduced the peak magnetic field strength in the gap--from 1.7 T to 1.5 T. We thus made a trade-off of beam deflection angle for event rate.

To facilitate the design of a fragment detection system and the analysis of data, the field of the modified magnet was mapped. The vertical component of the field was mapped with a hall probe over several horizontal areas of 96.5 cm x 164.6 cm on a grid size of 2.54 cm x 3.05 cm, resulting in 2184 points. The midplane of the magnet was mapped several times and averaged, and in addition, planes 2.54 cm below midplane, and 2.54, 2 x 2.54 and 3 x 2.54 cm above the midplane were mapped. The maps of planes 2.54 cm above midplane and 2.54 cm below midplane were compared to confirm the field's vertical symmetry about the midplane. Only the vertical component of the field was mapped over the entire field region. The other components were measured at representative points about the fringe fields, and their effects on the trajectories of fragments of interest were calculated. These non-vertical components were determined to have a negligible effect on the fragments to be studied, and were subsequently not mapped. With the vertical field maps we computed useful fragment trajectories; two are indicated in Figure 1.

3. Detector elements

A kinematically complete measurement of a dissociation event requires that we measure the energy and angle of all particles produced. Analysis of the experiment also requires an isotopic identification of each charged particle as well as a count of the total number of beam particles incident upon the target. A three-element array was developed to perform these tasks in conjunction with the beam-sweeping dipole. The first element is a pair of gas-filled parallel plate avalanche counters (PPAC's) [5]. They measure a projectile's position at two points upstream from the target, indicating its direction and point of intersection with the target. Although they are located at 0° in the beamline, these detectors are not a significant source of background reactions. The combined thickness of the two detectors is only ~ 1.4 mg/cm^2, compared to 250 - 400 mg/cm^2 thickness of the reaction targets. Also, the PPAC nearest the target is 1 meter upstream from the target, and so the neutron detectors subtend a much smaller solid angle for neutrons produced in the PPAC than they do for neutrons from the target. The probability of recording a coincidence event from a reaction in this PPAC is thereby diminished, and even more so for the most upstream PPAC. The second element of the system is a pair of Si strip detectors placed 15 cm downstream from the target, between the coils of the magnet. The detectors provide a measurement of the angle at which a fragment leaves the target. They also supply an energy loss measurement to be used for particle identification. The third portion of the system is a plastic scintillator array placed downstream from the exit of the magnet at an angle to the beam axis. The plastic array stops charged fragments produced in the target, measures their energies and gives a fast timing signal for use with the neutrons' detection. The array also stops and counts all beam particles which left the target unreacted. The Si strip detectors and the scintillator array are indicated in Figure1.

3.1 Silicon detectors

A geometry to minimize background would have only the target before the magnet, i.e., all detectors after the magnet. However, Si detectors placed after the magnet would be a considerable distance from the target and would, therefore, have to be very large to intercept all the fragments. They would be too expensive. Therefore, silicon strip detectors were placed 15 cm directly behind the target at 0°. While the silicon detectors are a source of background

events, their contribution relative to the target is much smaller than that made by the former zero-degree telescope. In a subsequent study of ^{11}Li dissociations with the dipole magnet, only15% of the events were created by reactions in the Si detectors.

The two Si strip detectors are 250 μm thick, cover an area of 5 cm x 5 cm each, and have sixteen 3-mm-wide horizontal strips which collect free electrons, while the other side has 16 vertical strips which collect electron holes. These strips effectively divide the detector into an array of 2 x 256 (x,y) pixels. The detectors are mounted 15 cm downstream from the target, directly between the coils of the magnet. At a distance of 15 cm from the target, a 3 x 3 mm pixel subtends an angle of approximately 1.2°.

A novel feature of these detectors is that, unlike conventional silicon strip detectors, which are framed on all four sides with a G-10 mount, the side of the frame opposite the cable connection is trimmed away from these detectors. Their active areas extend completely to one edge of each device so that, when aligned side by side, they actively cover a uniform 5-cm x 10-cm area. Figure 2 is a photograph of the strip detectors mounted on an ISO flange which bolts to the vacuum chamber.

The signals from the silicon strips are amplified by a set of MSU-constructed S800 pre-amps* and shaped by Washington-University-built, CAMAC controlled shapers [7]. The shaped signals are digitized by Philips peak-sensing ADCs, providing an energy loss measurement as well as x-y pixel information for an angle measurement. In addition to being shaped and digitized, the pre-amp signals are boosted by MSU-built quad fast amplifiers and processed by LeCroy CAMAC constant-fraction discriminators, providing a time signal from the detectors.

3.2 Scintillator array

After the silicon strip detectors, the remaining tasks to be performed by the fragment detection array are to stop and measure the total energy of the charged fragments, stop and count the unreacted beam particles and provide a fast timing signal for neutron velocity measurement. These tasks are accomplished with the use of a plastic scintillator array. The array is located outside the magnet, 1.7 m downstream from the target location, with its normal at an angle of 23.4 degrees to the beam axis. It consists of 16 vertical bars of Bicron BC-408 fast plastic scintillator, each 4 cm wide, 2 cm thick, and 40.64 cm long. A 2-inch photomultiplier tube

(PMT) views each end of each scintillator bar. The PMT's are Burle 8575 and Hamamatsu R329 tubes, with photocathode diameters of 46 mm. The 2-cm thickness of the scintillator bars is somewhat greater than the ranges of light fragments with energies of around 30 MeV/A. Given a 2 cm thickness, a 4 cm width was chosen for the bars so that the entire 2cm x 4cm cross-sectional area can be covered by the photocathode of the PMT without the use of a light pipe, as light pipes would have necessitated the construction of a taller vacuum chamber. Because the cross-sectional size of the PMTs is larger than that of the scintillators, the bars are staggered into two parallel planes, one plane 4.75 cm behind the other. This arrangement provides uniform and complete coverage of the exit plane of the magnet by the plastic array. The horizontal size of the array, 16x4=64 cm, is designed to stop both very rigid unreacted beams such as ^{8}He, as well as fragments such as ^{4}He which the magnet sweeps through a much larger angle. Because of the low magnetic rigidity of ^{4}He fragments, they do not travel all the way to the downstream end of the magnet before leaving the field area. Rather, they exit on the open side of the C-shaped magnet. Such a trajectory means that they travel a shorter distance between the poles of the magnet and, therefore see a larger vertical aperture defined by the poles. The height of the scintillator bars, 16 inches, is chosen to catch ^{4}He particles which emerge from between the magnet's poles at the maximum vertical angle. Figure 3 shows the scintillator bars and PM's as they are mounted in the vacuum chamber.

The surfaces of the scintillator bars have no reflecting material added, so that all scintillation light created within a cone of critical angle with respect to the scintillator surfaces is transmitted to the ends of the bars by total internal reflection. A memory of the vertical position of the fragment is thus retained. Approximately 60% of the scintillation light is emitted at angles less than the critical angle and escapes the bar, but 'cross-talk' effects in which the escaped light triggers neighboring phototubes is not found to be an important effect since light which escapes one bar cannot be captured by the walls of a neighboring bar. As light travels from its origin to each of the two phototubes by total internal reflection, the only losses are due to exponential attenuation by the plastic. The characteristic length of this absorption, 380 cm, is considerably longer than the 40 cm length of the scintillators. Still, to account for what attenuation occurs, the geometric mean of the two PMT signals is calculated. The mean of the two signals gives a pulse height which is independent of the position of the source of the light.

---

* Amaxis Systems, Inc., 2817 Olde Gloucester, St. Charles, MO 63301

The PMTs are biased and read out by high voltage bases built at the NSCL. The bases are modified versions of the Hamamatsu model E394 base. The first modification to the Hamamatsu design is that the resistors in the NSCL version have half the resistance of the Hamamatsu version. This doubles the bleeder current through the device, helping to retain linearity for large pulses. The second modification is that the bases are split into two separate modules. Inside the vacuum chamber a socket device containing the capacitive portion of the circuit is connected directly to the PMTs. These sockets are connected via ribbon cable feed-throughs to the resistor chains on the outside of the vacuum chamber. The voltage dividers are placed outside the vacuum to dissipate heat generated in the resistors, preventing gain drifts from resistive heating, and damage to the system caused by excessive heating of the bases. Two signals are pulled from each phototube base. In addition to the anode pulse, which is integrated by a charge-to-digital converter for an energy measurement, a signal from the eleventh of the twelve dynodes is inverted and used for timing purposes.

To monitor what gain drifts do occur, a blue light-emitting diode is fixed to the face of each PMT. The LEDs are fired at a rate of one pulse per second throughout the experiment, and the resulting PMT signals are recorded along with the experimental data. Offline analysis showed that over the course of a several-week experiment the gain drifts of the PMTs were negligible compared to the resolution of the scintillator array.

4. Vacuum chamber

The last piece of equipment constructed for use with the beam-sweeping dipole is a vacuum chamber to contain the detectors and couple the system to the beamline. The chamber was made of stainless steel rather than aluminum because its strength allowed the chamber to be constructed with thinner walls, maximizing the vertical aperture of the chamber between the poles of the magnet. The vacuum chamber consists of three regions. The first region couples to the beamline and fits between the poles of the magnet. Like the rest of the chamber, it is constructed of 0.635-cm walls, so the interior height of the chamber between the poles is 17.8 cm. The next section of the chamber begins at the exit of the magnet and has an interior height of 41.9 cm, to allow fragments to see the entire vertical height of the scintillator bars. The last section of the vacuum chamber houses the scintillator array and is 91.4 cm tall to accommodate the plastic bars and their phototubes.

The far upstream end of the vacuum chamber is coupled to the beamline through a gate valve. In the beamline is a pair of gas-filled PPACs used to measure the incoming beam particles' directions. PPAC detectors are damaged by rapid pressure changes, and so the gate valve can be closed to isolate the chamber from the beamline, allowing rapid pump down and venting of the chamber while the PPACs stay in the vacuum of the beamline. Between the gate valve and the magnet are vertical lengths of pipe extending above and below the chamber. A large target ladder, capable of holding 7 reaction targets 5.1 cm high and 7.6 cm wide is mounted in the pipe. The target ladder is manipulated by a push rod that can be run up or down by hand to change the target.

Between the coils of the magnet, 15.2 cm downstream from the target ladder, are located the Si strip detectors. The detectors are mounted on an aluminum rail that is bolted to an ISO flange on one side of the chamber. The flange includes feed-throughs for all cable connections to the detectors and can be quickly removed and replaced with a standard blank-off for work in the chamber that does not involve the silicons. A mounting rack for the Si preamps is clamped to the chamber to ensure a solid ground between the vacuum chamber and the preamp cases. When bolted into place, the preamps are suspended directly in front of the feed-through flange, allowing the cables between the preamps and the flange to be only a few cm long, minimizing their tendency to pick up noise.

The performance of Si detectors may be impaired by thermal noise. Our detectors are placed between the coils of a room temperature magnet that becomes considerably warmer than room temperature when operating. In test runs with the device, we found that as the magnet coils warmed the vacuum chamber, radiative heating of the silicons from the chamber walls quickly increased the leakage current of the detectors and impaired their resolution. To prevent such heating, a copper shroud was built and installed inside the chamber between the pole faces, shielding the detectors from the warm surfaces of the vacuum chamber. The shroud is a box with a rectangular opening for the beam particles to enter, and the entire downstream end is open for fragments to leave the detector over a large range of angles. The shroud is insulated from the vacuum chamber by ceramic feet, and copper lines are soldered onto its surface. Cold domestic water flows through the lines, cooling the shroud and shielding the Si detectors from the warm chamber walls. When the magnetic field is ramped up or down, eddy currents in the copper

shroud tend to pull it around the chamber. To fix it in place, two stainless steel studs were welded to the chamber, and the shroud was bolted down.

Immediately outside the magnet's coils, both on the open side of the magnet and the downstream end, is the junction between the first and second regions of the vacuum chamber. With an inside height of 41.9 cm, the second region of the chamber allows charged particles created in the target to see the entire height of the scintillator array. This portion also is constructed of 0.635-cm stainless steel, with the exception of a neutron exit window, centered at zero degrees on the back wall of the chamber. To minimize scattering of the target neutrons in flight to the Neutron Walls, this window is made from a plate of aluminum Hex-Cel honeycomb material, which is bolted to the chamber with an aluminum frame and sealed with an O-ring. Though it is strong enough to support the atmospheric load of the vacuum, the 49.5 cm x 66.0 cm the mass of the window is only 6.6 kg, compared to 79 kg for a stainless steel sheet of similar dimensions.

The third and final portion of the vacuum chamber is a box which houses the plastic scintillator array. The back wall of this section of the chamber is a 1.9-cm-thick aluminum plate bolted to the chamber and sealed with an O-ring. The scintillator array is mounted on this plate, so that the entire assembly can be removed from the chamber in one piece and the plate replaced with a blank-off for work not requiring the scintillators.

The purpose of the magnet is to prevent neutrons produced in the fragment detectors from reaching the Neutron Walls. Although a 21 MeV/A ^{11}Li beam is bent by an angle of 22° before stopping in the plastic, the sweeping of the beam alone is not enough to ensure that no neutrons from the detectors will reach the Walls. Using the maps of the magnetic fields, the trajectories of unreacted beam particles are calculated through the magnet to determine where they strike the scintillator array. Outside the vacuum chamber, directly behind the plastic array, a stack of brass and steel shielding is assembled to absorb detector neutrons as they exit the chamber. In the first experiment, this shield was 20 cm thick. While it greatly reduced the flux of neutrons from the plastic array to the Walls, the data contained a significant number of ^{9}Li-1n coincidences that were the result of reactions in the scintillators. However, because of the absorption of neutrons by the shielding, the set of ^{9}Li-2n coincidences showed an insignificant contamination from detector events. For subsequent experiments, the thickness of the stack was increased to 30 cm. In addition, brass bars 5 cm thick were bolted to the inside of the aluminum detector plate a few

cm behind the scintillators. The additional shielding essentially eliminates fragment-1n coincidences resulting from reactions in the plastic array.

5. Operation of the system

5.1 Energy measurement

The scintillator array is calibrated by using the NSCL A1200 Spectrograph to create a beam of fragments of the type that will be measured in the experiment. The field of the dipole magnet is adjusted to sweep the beam over the scintillator array, illuminating as many bars as the bending power of the magnet permits. Unfortunately, the pulse height of scintillation light produced in the plastic bars is not directly proportional to the amount of energy deposited in the detector by the fragment. For our purposes, an acceptable parameterization of the light production is achieved by the method developed by D. Cebra, *et al.* [8]. All detectors are gain matched, and then the pulse height is converted into light intensity in units of MeV electron equivalent (MeVee) by the equation:

$$L=0.265(E^{1.39}/Z^{0.78}A^{0.41})$$

where E is the total energy of the fragment in MeV, and Z and A are the atomic and mass numbers of the fragment. For each calibration beam, the measured pulse height is plotted against the calculated light production for that isotope and energy. The points are fitted with a line, and the fit is used to convert from pulse height to fragment energy. Shown in Figure 5 is the calibration curve of pulse height to light intensity for one scintillator bar illuminated by several fragment beams, as well as the response of that bar to a calibration beam of ^{9}Li particles. For ^{9}Li particles of 23.4 MeV/A, an energy resolution of 1.4%, FWHM was achieved.

5.2 Particle identification

Isotopic identification of charged fragments and beam particles is achieved by the ΔE-E method. For each particle, the energy loss measured by the Si detectors is plotted against the total energy measured by the silicon and the plastic bars. Figure 6a is a ΔE-E plot measured between the Si strips and the scintillator array in a ^{11}Li experiment.

The ΔE-E spectra from bars which stopped the ^{11}Li beam show some contamination between the ^{9}Li and ^{11}Li regions of the plots. A plot of the total energy spectrum from a

scintillator bar which stopped only ^{9}Li particles (Fig. 5, bottom) shows a symmetric, gaussian-shaped peak centered at the expected energy. The energy spectrum from a bar which stopped ^{11}Li beam particles, however, shows a single peak at the expected energy with an asymmetric low energy tail. This low energy tail is responsible for the contamination between the two nuclei in the ΔE-E plot. That contamination is caused by ^{11}Li projectiles which lost various fractions of their energy in the scintillator before dissociating and liberating two neutrons. (With a 2n separation energy of only 0.3 MeV, ^{11}Li readily dissociates into ^{9}Li + 2n.) The neutrons then carried off energy not detected by the scintillator, yielding a lower than normal energy measurement for that particle. Our system is designed to detect such dissociation events when they occur in a target, but the shielding blocks behind the scintillator bars prevent scintillator-liberated neutrons from reaching the neutron detectors. When a coincidence with two neutrons was required, the energy spectrum from a bar showed no low energy tail. A plot of ΔE-E for these events is shown in Figure 6b, and the ^{9}Li region is more sharply defined.

5.3 Time-of-flight reference

To perform a time-of-flight (TOF) measurement of neutrons detected in the Neutron Walls, the fragment detection system must also provide a reference time signal which can be used to determine when the neutrons and fragment left the reaction target. Ideally, this signal would come from the silicon strip detectors, as the 15-cm flight path between target and detector would require a negligible correction for the fragments' flight times with varying energy. However, in the vicinity of the dipole magnet power supplies, the fast outputs of the silicon pre-amps are prone to noise-pickup problems, and the system is unstable. A more reliable time signal is obtained from the dynode signals of the plastic array PMTs. To compensate for the varying transit times of light from different source points in a scintillator bar, the average of the time signals from each bar's two PMTs is calculated. The inherent timing resolution of the scintillator bar-Neutron Wall combination is illustrated by events in which the primary beam reacts in the plastic of the fragment array, creating γ rays which are detected by the Neutron Walls. A TOF spectrum for γ rays created by an ^{18}O beam in the bars is shown in Figure 7. There are six channels per nanosecond, and the resolution of the γ-ray peak is 0.8 ns, FWHM.

In addition to the γ-ray spectrum shown above, the timing of the scintillator array -- Neutron Wall system is calibrated with a ^{60}Co γ-ray source. The source is positioned inside the

vacuum chamber near the Si detectors, and γ-γ coincidences are recorded between the 16 scintillator bars and the 48 cells of the Neutron Walls. Because of the small pulse height of these events, the time resolution of the ^{60}Co coincidence spectrum is inferior to the spectrum from beam-induced γ rays produced in the scintillators. However, a long acquisition time with the source provides excellent statistics, and even with a resolution of 3.5 ns, FWHM, these data provide adequate time calibration for bars which stopped low numbers of beam particles, and show no beam induced γ ray peak. Figure 8 shows a ^{60}Co timing calibration for one scintillator bar vs. the 24 cells of a Neutron Wall.

When measuring the TOF of neutrons and γ rays created in the target, the time signal from the bars is used as the neutron TOF stop. However, the raw time signal from the bars is not a proper TOF stop, because fragments of varying energy will have a range of flight times from the target to the scintillator bars, introducing an error in the measurement of neutrons' flight times from target to the Neutron Walls. These fragment flight times must be calculated on an event-by-event basis, and used to correct the measured neutron times-of-flight. Using the magnetic field maps, a fragment's trajectory can be calculated through the magnet using a fourth-order Runge-Kutta integration routine, as described in standard references.[9] The scintillators are positioned with respect to the magnet such that, over a broad range of energy and incident angle, the flight path between the target and the front surface of the plastic array is nearly constant for a fragment of a given isotope. For ^{9}Li fragments varying in energy from 20 to 30 MeV/A and in angle into the magnet from –10° to +10°, the flight paths from the target to the front of the plastic array differ by less than 2 cm, corresponding to 0.3 ns. While no correction, therefore, is necessary for a fragment's energy or angle, an additional 4.75 cm of flight path length is added for events in which the fragment is detected by bars in the second row of the staggered array (see Figure 3.) After a fragment's energy is determined from the size of the light pulse, its velocity and TOF from target to detector are calculated, and that time is added to the neutron TOF measurement. This is done for each event.

6. Acknowledgements

We acknowledge Dr. Rich Tighe for his help in securing the dipole magnet from Lawrence Berkeley Laboratory, and we thank Jim Vincent for the construction of the PMT bases and divider chains. We are also indebted to Doug Harris, Jon Brandon and Harold Hilbert for

help with construction and installation of the magnet system. We are grateful for the support of the National Science Foundation under Grant No. PHY 95-28844, as well as the Ministry of Education, Science, Sports, and Culture of Japan under Grant Nos. 08044095 and 08640392.

References

[1] R. Anne, S.E.Arnell, R. Bimbot, H. Emling, D. Guillemaud-Mueller, P.G. Hansen, L. Johannsen, B. Jonson, M. Lewitowicz, S. Mattson, A.C. Mueller, R. Neugart, G. Nyman, F. Pougeon, A. Richter, K. Riisager, M.G. Saint-Laurent, G. Schrieder, O. Sorlin, and K. Wilhelmsen, Phys. Lett. B 250 (1990) 19.

[2] D. Sackett, K. Ieki, A. Galonsky, C.A. Bertulani, J.J. Kruse, W.G. Lynch, D.J. Morrissey, N.A. Orr, H. Schulz, B.M. Sherrill. A. Sustich, J.A. Winger, F. Deak, A. Horvath, A. Kiss, Z. Seres, J.J. Kolata, R.E. Warner, and D.L. Humphrey, Phys. Rev. C 48 (1993) 118.

[3] K. Ieki, D. Sackett, A. Galonsky, C.A. Bertulani, J.J. Kruse, W.G. Lynch, D.J. Morrissey, N.A. Orr, H. Schulz, B.M. Sherrill. A. Sustich, J.A. Winger, F. Deak, A. Horvath, A. Kiss, Z. Seres, J.J. Kolata, R.E. Warner, and D.L. Humphrey, Phys. Rev. Lett. 70 (1993) 730.

[4] D. Sackett Ph.D. Thesis, Michigan State University (1992)

[5] D. Swan, J. Yurkon, D.J. Morrissey, Nucl. Instr. & Meth. A348, (1994) 314.

[6] P.D. Zecher, A. Galonsky, J.J. Kruse, S.J. Gaff, J. Ottarson, J. Wang, F. Deak, A. Horvath, A. Kiss, Z. Seres, K. Ieki, Y. Iwata and H.R. Schelin, Nucl. Instr. & Meth. A401 (1997) 329.

[7] B. Davin et al., Nuclear Instruments and Methods in Physics Research , to be submitted.

[8] D. Cebra, W.K. Wilson, A. Vander Molen and G.D.Westfall, Nucl. Instr. & Meth. **A313** (1992) 367.

[9] W. Press, S. Teukolsky, W. Vetterling, B. Flannery, *Numerical Recipes in Fortran, Second Edition* (Cambridge University Press, Victoria Australia, 1992) p. 704.

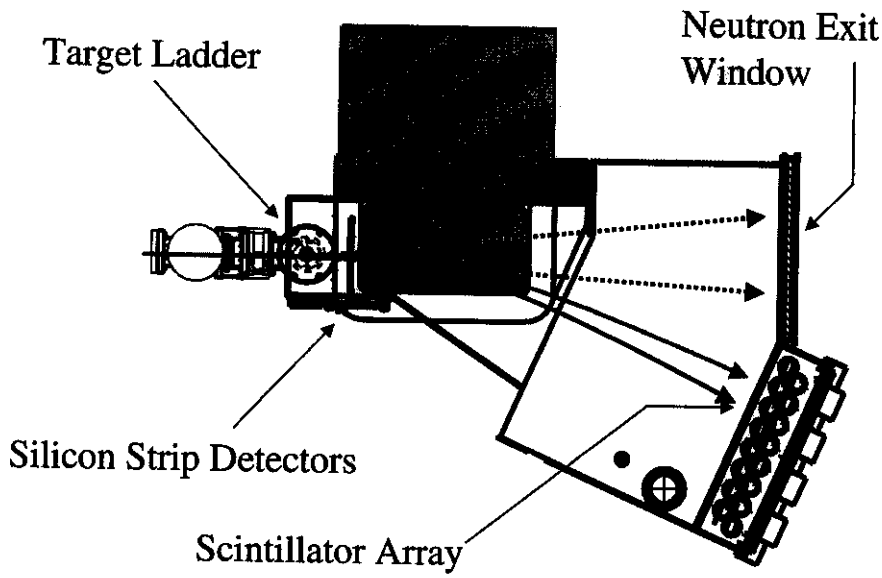

Figure 1 -- Diagram of the Beam Sweeping Dipole, its vacuum chamber, and associated detectors. The beam enters the chamber from the left. Not shown are the position sensitive PPAC detectors, upstream from the target. The grey curve shows the path of an unreacted ^{11}Li particle through the magnet, while the solid black curve shows the path of a ^{9}Li fragment created in the target. The dotted lines represent the paths of two neutrons produced in coincidence with the ^{9}Li.

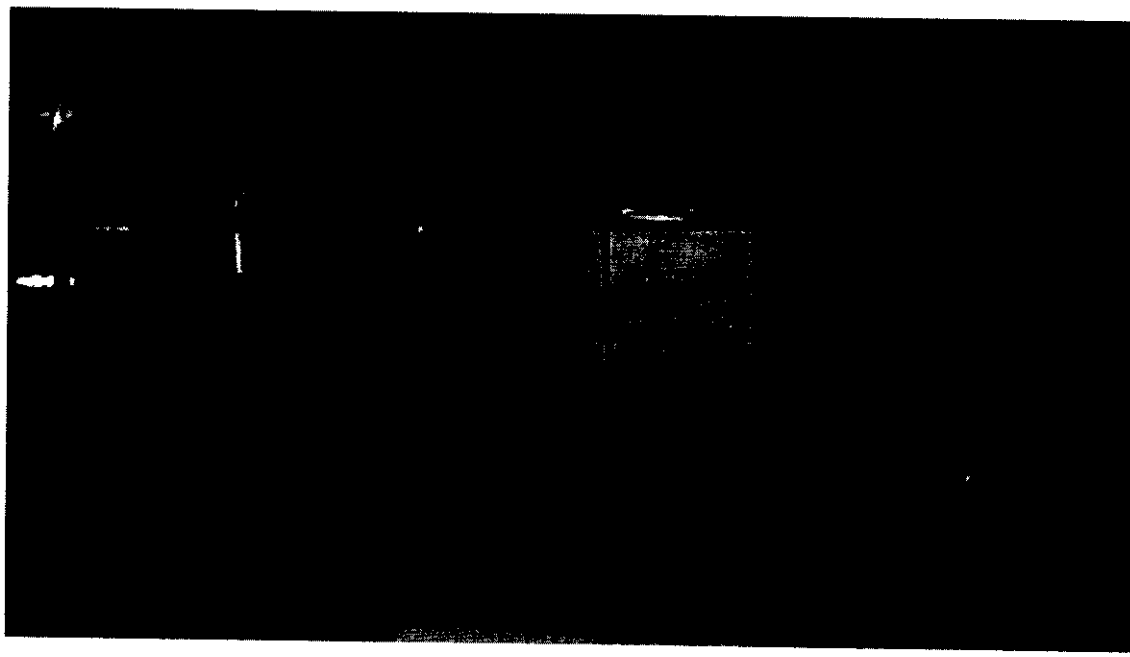

Figure 2 -- The silicon strip detectors. The 3-mm horizontal strips are visible on the front surfaces. The flange at left bolts to the vacuum chamber to suspend the detectors at zero degrees behind the target.

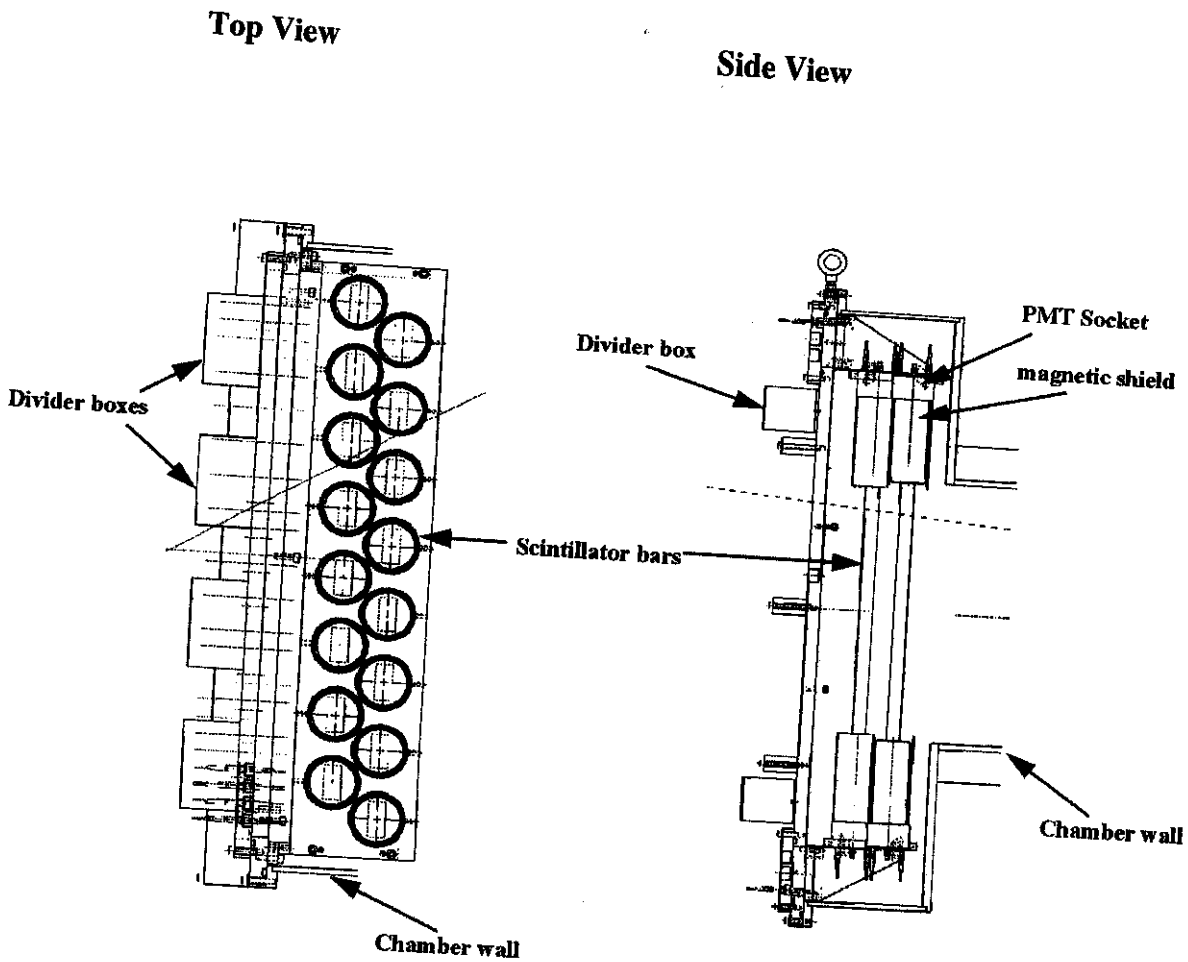

Figure 3 -- CAD drawings of the plastic scintillator array at the exit of the Beam Sweeping Dipole.

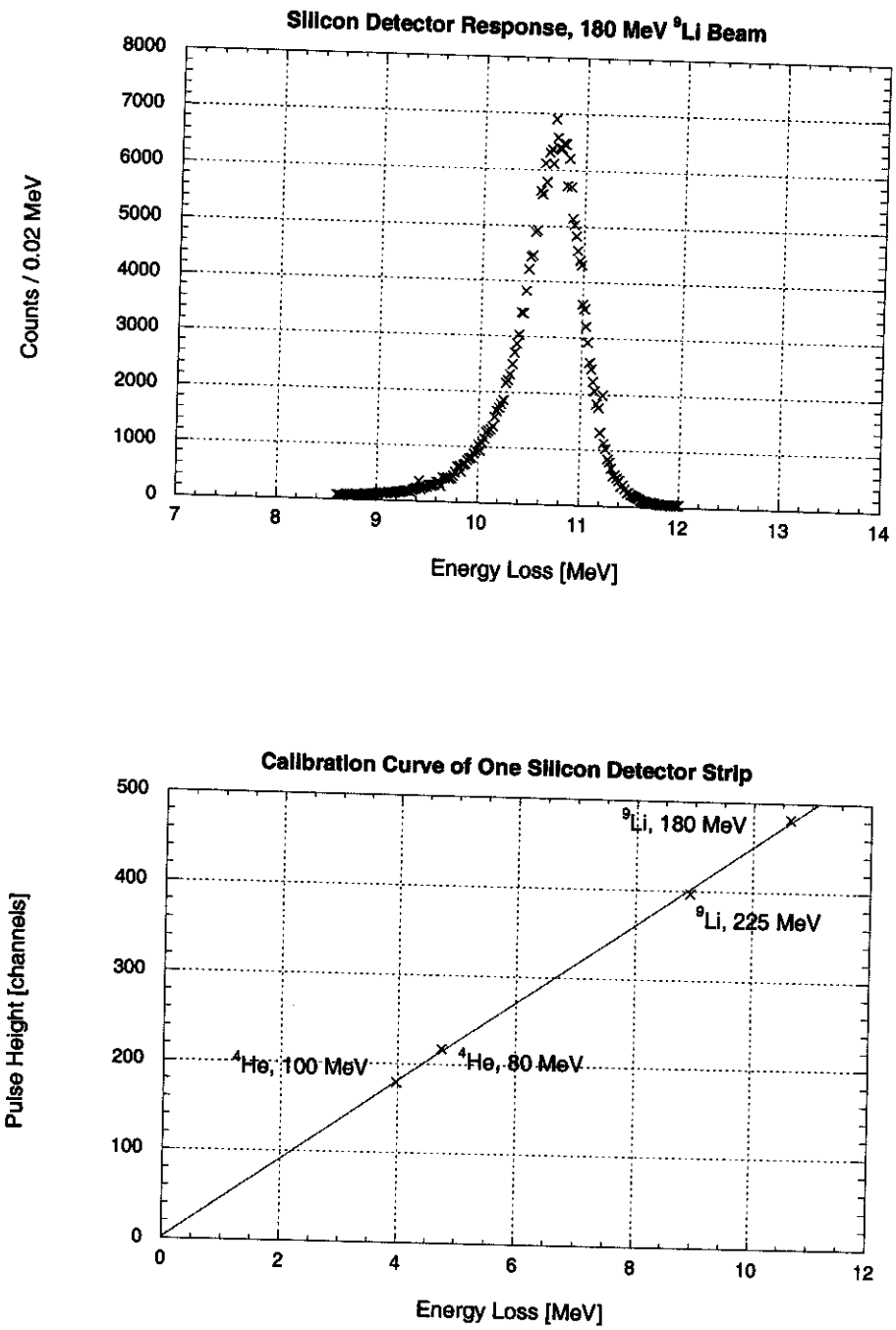

Figure 4 -- Detector response and calibration of silicon strip detectors

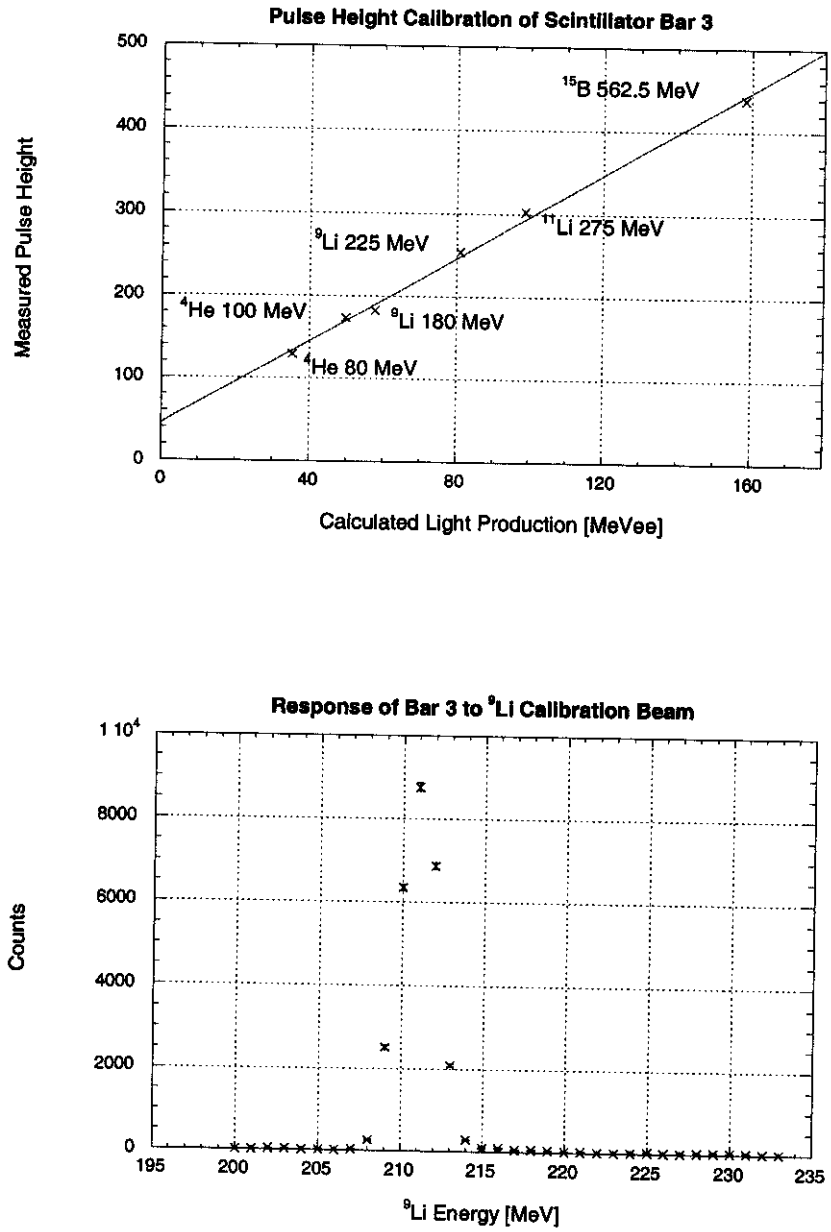

Figure 5 -- Top: Pulse height measured in scintillator bar 3 vs. calculated light production for each calibration beam, as well as a number of experimental beams. Bottom: Pulse height resolution of bar 3 in response to a 211 MeV ^{9}Li calibration beam. The width of the peak is 1.4% FWHM.

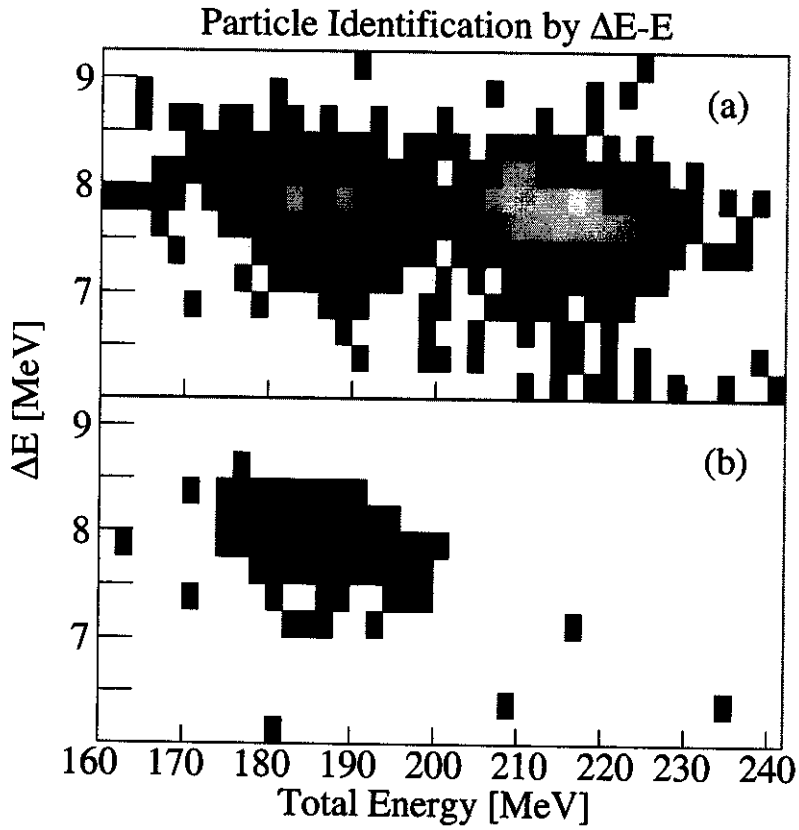

Figure 6 -- ΔE-E plots from ^{11}Li experiment. Only the region around ^{11}Li and ^{9}Li is shown. a) ^{9}Li and ^{11}Li for all event types, including fragment singles as well as fragment-1n and fragment-2n coincidences. b) Particle identification plot for fragment – 2n coincidences only.

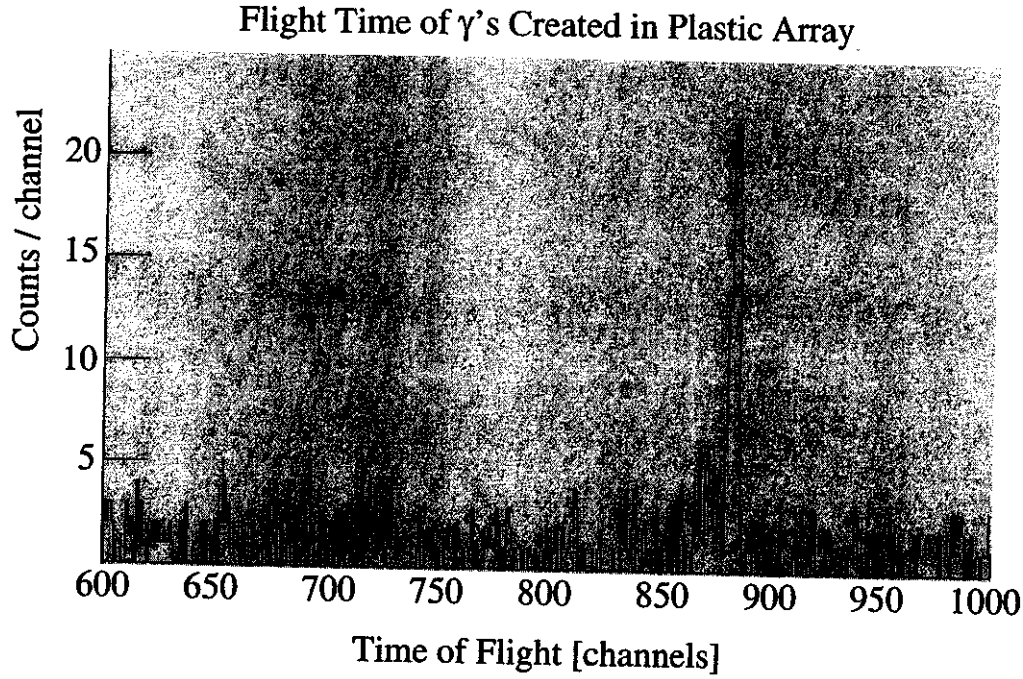

Figure 7 -- TOF of γ-rays created in scintillator bars by a beam of ^{18}O and detected by the Neutron Walls. The peak has a resolution of 0.8 ns, FWHM.

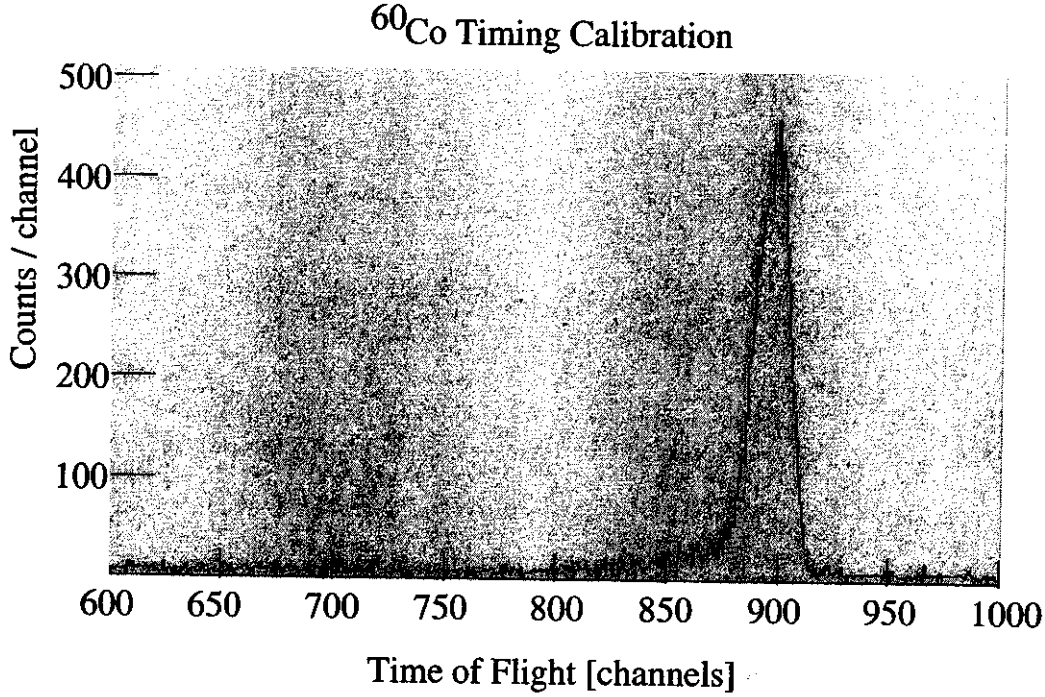

Figure 8 -- ^{60}Co timing calibration for one bar vs. front Neutron Wall. The peak has a resolution of 3.5 ns, FWHM.